The Journal of Chemical Physics

Joint refinement model for the spin resolved one-electron reduced density matrix of $YTiO_3$ using magnetic structure factors and magnetic Compton profiles data

Cite as: J. Chem. Phys. **148**, 164106 (2018); https://doi.org/10.1063/1.5022770
Submitted: 18 January 2018 • Accepted: 28 March 2018 • Published Online: 26 April 2018

Saber Gueddida, Zeyin Yan, Iurii Kibalin, et al.

Joint refinement model for the spin resolved one-electron reduced density matrix of $YTiO_3$ using magnetic structure factors and magnetic Compton profiles data

Saber Gueddida,[1,a)] Zeyin Yan,[1] Iurii Kibalin,[2] Ariste Bolivard Voufack,[2] Nicolas Claiser,[2] Mohamed Souhassou,[2] Claude Lecomte,[2] Béatrice Gillon,[3] and Jean-Michel Gillet[1,b)]
[1]*SPMS, UMR8580, CentraleSupelec, Université Paris-Saclay, 3 Rue Joliot-Curie, Gif-sur-Yvette 91190, France*
[2]*CRM², Institut Jean Barriol, Université de Lorraine and Centre National de la Recherche Scientifique, BP239, F54506 Vandoeuvre-lès-Nancy, France*
[3]*Laboratoire Léon Brillouin, CEA, Centre National de la Recherche Scientifique, CE-Saclay, 91191 Gif-sur-Yvette, France*

(Received 18 January 2018; accepted 28 March 2018; published online 26 April 2018)

In this paper, we propose a simple cluster model with limited basis sets to reproduce the unpaired electron distributions in a $YTiO_3$ ferromagnetic crystal. The spin-resolved one-electron-reduced density matrix is reconstructed simultaneously from theoretical magnetic structure factors and directional magnetic Compton profiles using our joint refinement algorithm. This algorithm is guided by the rescaling of basis functions and the adjustment of the spin population matrix. The resulting spin electron density in both position and momentum spaces from the joint refinement model is in agreement with theoretical and experimental results. Benefits brought from magnetic Compton profiles to the entire spin density matrix are illustrated. We studied the magnetic properties of the $YTiO_3$ crystal along the Ti–O_1–Ti bonding. We found that the basis functions are mostly rescaled by means of magnetic Compton profiles, while the molecular occupation numbers are mainly modified by the magnetic structure factors. *Published by AIP Publishing.* https://doi.org/10.1063/1.5022770

I. INTRODUCTION

Transition metal perovskites have attracted considerable attention during the last decades and exhibit a wide range of physical properties, such as superconductivity, ferromagnetism, and ferroelectricity. These materials are characterized by narrow 3*d* bands and strong Coulomb correlations. The physical properties of perovskite oxides ABO_3 are extremely sensitive to the radius size of atom A (where A = Gd, Sm, Y, ..., La); the strontium and calcium vanadate are correlated metals, while the lanthanum and yttrium titanate are Mott insulators with gaps of 0.2 and 1 eV, respectively.[1–3] In this work, we studied yttrium titanate ($YTiO_3$) because it is a rare example of a Mott-Hubbard insulator with a ferromagnetic ground state below a Curie temperature of 30 K.[4] $YTiO_3$ has an orthorhombic crystal structure Pnma and a single *d* electron in the t_{2g} orbital of each Ti atom. The t_{2g} orbitals have a much stronger localized character due to the weak *p*–*d* interaction.[5] The crystal structure of $YTiO_3$ has been investigated theoretically[6–8] and by different experimental techniques.[5,9–16]

Recently, the unpaired 3*d* electron distribution of Ti atoms has been investigated by means of polarized neutron (PN) diffraction[17] and directional magnetic Compton (MC) scattering.[18] The polarized neutron diffraction[19–26] gives access to the spin density in position space, while the directional magnetic Compton scattering[23,25,27,28] reflects the momentum distribution of the unpaired electron in momentum space. In both studies, i.e., in both spaces, the computed (full periodic calculation) and measured spin densities compare very well.[17,18] In the position space, a small magnetic moment is observed on oxygen O_1 of the $YTiO_3$ crystal, which is significant to explain the role of this atom in mediating magnetic interactions between neighboring Ti coordination polyhedra.[17] This confirmed that magnetic interactions between the neighboring Ti t_{2g} orbitals are governed by the superexchange process mediated by the O_{2p} orbitals. On the other hand, the reconstructed momentum spin density shows that the Ti–O_1–Ti path plays a major role in the spin delocalization and the ferromagnetic coupling of metallic sites.[18] Therefore, we deduced that the magnetic properties of the $YTiO_3$ compound are mainly localised along the Ti–O_1–Ti pathway.

In previous studies,[17,18] the position and momentum spin densities were reconstructed separately using experimental magnetic structure factors (MSFs) and magnetic Compton profiles (MCPs), respectively. In the present work, the spin electron distributions in both spaces, i.e., the entire spin-resolved one-electron-reduced density matrix[29–36] (1-*SRDM*) elements, are **simultaneously** reconstructed from the theoretical MSFs and MCPs using the joint refinement model.[37] The aim of the present work is therefore to (1) reproduce the magnetic and electronic properties of a $YTiO_3$ crystal from a simple molecular model with limited basis sets and (2) assess the added value of the combination of MSFs and MCPs to reconstruct the entire 1-*SRDM*.

[a)]Electronic mail: saber.gueddida@centralesupelec.fr
[b)]Electronic mail: jean-michel.gillet@centralesupelec.fr

The joint refinement procedure[37] is based on four main stages: first, modeling a cluster using a standard molecular *ab initio* package and second, from the resulting wavefunction, the MSFs and the MCPs are computed. Third, the basis function extensions are optimised by modifying the exponent coefficients for each atomic orbital to better match pseudo-experimental data. Finally, the spin population matrix is also adjusted by varying the molecular orbital occupation numbers. The refinement of a 1-*SRDM* to the pseudo-experimental data plays a central role in the description of electronic properties and provides important information on chemical bonding.[19,20,27]

This model has been tested previously on an artificial magnetic crystal of urea with two different interaction molecular distances.[37] It has been shown that the joint refinement model gives more accurate results than the refinement on the MSFs only. This test of feasibility confirms that the MSFs mostly improve the diagonal elements of the 1-*SRDM*, but do not allow a description of very fine details of the spin distributions over the entire 1-*SRDM*. However, the 1-*SRDM* is strongly affected by the MCP information not only on its off-diagonal regions but also on its diagonal regions.

This paper is organized as follows: in Sec. II, we recall the different stages of the joint refinement model and describe the generation of pseudo-experimental data from periodic calculations of $YTiO_3$. In Sec. III, we present and discuss the results of the molecular model $(Ti_2O)_2$ and compare them to the periodic computation reference. Finally, conclusions are given in Sec. IV.

II. COMPUTATIONAL PROCEDURE

The molecular model considered in this work contains two fragments of Ti–O_1–Ti bonds [noted $(Ti_2O)_2$]. We wish to test the ability of the joint refinement model to reproduce the electronic and the magnetic properties of the $YTiO_3$ crystal using such a simple cluster model absorbing information from two data sets from two pseudo-experiments: polarized neutron diffraction and directional magnetic Compton scattering. These two techniques are highly complementary and give a more complete physical picture of the entire 1-*SRDM*. $YTiO_3$ crystallizes in the orthorhombic space group Pnma (see Fig. 1, left) and is often used as an example of a Mott-Hubbard insulator with a ferromagnetic ground state. The corresponding lattice parameters are set to a = 5.690 Å, b = 7.609 Å, and c = 5.335 Å. The nominal ionic charges of Y, Ti, and O are taken to be 3, 3, and −2, respectively. The present cluster model contains two fragments; each one is built from two Ti atoms linked by an O_1 atom along the crystallographic *b* direction. The remaining O and Y atoms are replaced by point charges (see Fig. 1, right). The molecular calculation was performed at the Hartree-Fock level with a minimal basis set 6-31G.[38–46]

The joint refinement model[37] is implemented as a post-processing of a molecular *ab initio* package based on a LCAO approach (in this work, the GAUSSIAN package[47]). Therefore, the molecular orbitals are expressed as a linear combination of Gaussian functions as follows:

$$\begin{aligned}\Phi_i(\mathbf{r}) &= \sum_{j=1} C_{i,j}\chi_j(\mathbf{r}),\\ &= \sum_{j=1} C_{i,j}\sum_{k=1} d_{j,k}N(\alpha_k)(x-A_{x_k})^{a_k}(y-A_{y_k})^{b_k}\\ &\quad\times(z-A_{z_k})^{c_k}e^{-\alpha_k(\mathbf{r}-\mathbf{R}_k)^2},\end{aligned} \tag{1}$$

where $C_{i,j}$ are the molecular orbital coefficients, $d_{j,k}$ are the contraction coefficients of the *j*th orbitals and their corresponding *k*th Gaussian functions, and a_k, b_k, and c_k control the angular momenta *L*, where $L = a_k + b_k + c_k$. $A_{x_k}, A_{y_k}, A_{z_k}$ are the coordinates of the atomic position $\mathbf{R}_k$. Using expression (1), the 1-*RDM* can be expressed in terms of molecular orbitals $\Phi_i(\mathbf{r})$ and their respective occupation numbers n_i, which represent the eigenfunctions and eigenvalues, respectively,

$$\Gamma^{(1)}(\mathbf{r},\mathbf{r}') = \sum_{i=1} n_i\Phi_i(\mathbf{r})\Phi_i(\mathbf{r}'). \tag{2}$$

Using expressions (1) and (2), the 1-*SRDM* can be expressed as a functional of a spin population matrix and the product of two basis functions (χ),

$$\Gamma_s^{(1)}(\mathbf{r},\mathbf{r}') = \Gamma_\uparrow^{(1)}(\mathbf{r},\mathbf{r}') - \Gamma_\downarrow^{(1)}(\mathbf{r},\mathbf{r}') = \sum_{j,k} P_{j,k}\chi_j(\mathbf{r})\chi_k(\mathbf{r}'), \tag{3}$$

where the spin population matrix is given by

$$P_{j,k} = \sum_{i=1} n_i^\uparrow C_{i,j}^\uparrow C_{i,k}^\uparrow - \sum_{i=1} n_i^\downarrow C_{i,j}^\downarrow C_{i,k}^\downarrow. \tag{4}$$

It is well-known that the MSFs are Fourier transforms of the spin density in position space, which corresponds to the diagonal elements of 1-*SRDM*. Therefore, the MSFs can be

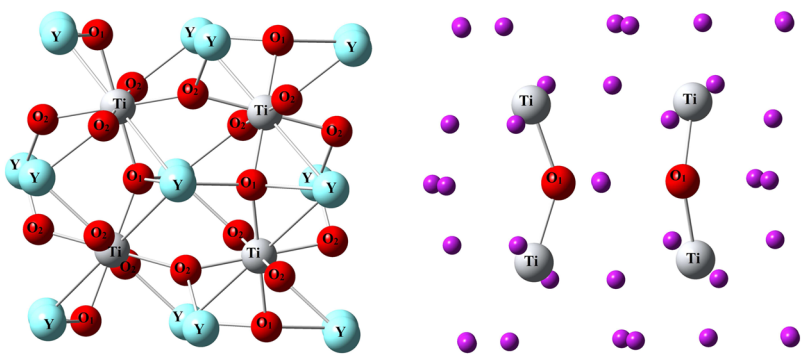

FIG. 1. Left panel: The crystal structure of $YTiO_3$. Lattice parameters are set to a = 5.690 Å, b = 7.609 Å, and c = 5.335 Å. Right panel: The cluster model contains two fragments of Ti–O_1–Ti and atoms in the immediate vicinity have been replaced by point charges.

expressed as follows:

$$F_M(\mathbf{Q}) = \int \Gamma_s^{(1)}(\mathbf{r},\mathbf{r}) e^{i\mathbf{Q}\cdot\mathbf{r}} d\mathbf{r} = \sum_{j,k} P_{j,k} \int \chi_j(\mathbf{r})\chi_k(\mathbf{r}) e^{i\mathbf{Q}\cdot\mathbf{r}} d\mathbf{r}. \tag{5}$$

The off-diagonal elements of 1-*SRDM*, which are connected to the spin density in momentum space, are related to the MCPs via

$$J(\mathbf{u},q) = \frac{1}{2\pi} \sum_{j,k} P_{j,k} \iint \left[\int S_{j,k}(\mathbf{r}) e^{-i\mathbf{p}\cdot\mathbf{r}} d\mathbf{r} \right] e^{i\mathbf{p}\cdot\mathbf{u}t} d\mathbf{p} e^{-iqt} dt, \tag{6}$$

where

$$S_{j,k}(\mathbf{r}) = \int \chi_j(\mathbf{r}')\chi_k(\mathbf{r}'+\mathbf{r}) d\mathbf{r}'. \tag{7}$$

The second stage of the joint refinement model consists in rescaling the basis functions (denoted "Dzeta refinement") by optimising the exponent coefficient of each atomic orbital $\{\alpha\} \Rightarrow \{\alpha_0\} \times \zeta_j$, where $0.8 \lesssim \zeta_j \lesssim 1.2$ to match the pseudo-experimental data. A subsequent normalization of the modified basis functions is performed by the molecular *ab initio* code (in this work, the GAUSSIAN package[47]). Therefore, from (1) the rescaled basis function of each atomic orbital j is expressed as a follows:

$$\chi_j(\zeta_j,\mathbf{r}) = \sum_{k=1} d_{j,k} N(\zeta_j\alpha_{0,k})(x-A_{x_k})^{a_k}(y-A_{y_k})^{b_k} \times (z-A_{z_k})^{c_k} e^{-\zeta_j\alpha_{0,k}(\mathbf{r}-\mathbf{R}_k)^2}, \tag{8}$$

where $\alpha_{0,k}$ is the initial exponent coefficient of the kth Gaussian function. By inserting expression (8) into expressions (5) and (6), the variation of the basis functions can clearly be seen in the expression of the MSFs,

$$F_M(\mathbf{Q}) = \sum_{j,k} P_{j,k} \int \chi_j(\zeta_j,\mathbf{r})\chi_k(\zeta_k,\mathbf{r}) e^{i\mathbf{Q}\cdot\mathbf{r}} d\mathbf{r}, \tag{9}$$

and the MCPs,

$$J(\mathbf{u},q) = \frac{1}{2\pi} \sum_{j,k} P_{j,k} \iint \left[\int S_{j,k}(\{\zeta\},\mathbf{r}) e^{-i\mathbf{p}\cdot\mathbf{r}} d\mathbf{r} \right] \times e^{i\mathbf{p}\cdot\mathbf{u}t} d\mathbf{p} e^{-iqt} dt, \tag{10}$$

where

$$S_{j,k}(\{\zeta\},\mathbf{r}) = \int \chi_j(\zeta_j,\mathbf{r}')\chi_k(\zeta_k,\mathbf{r}'+\mathbf{r}) d\mathbf{r}'. \tag{11}$$

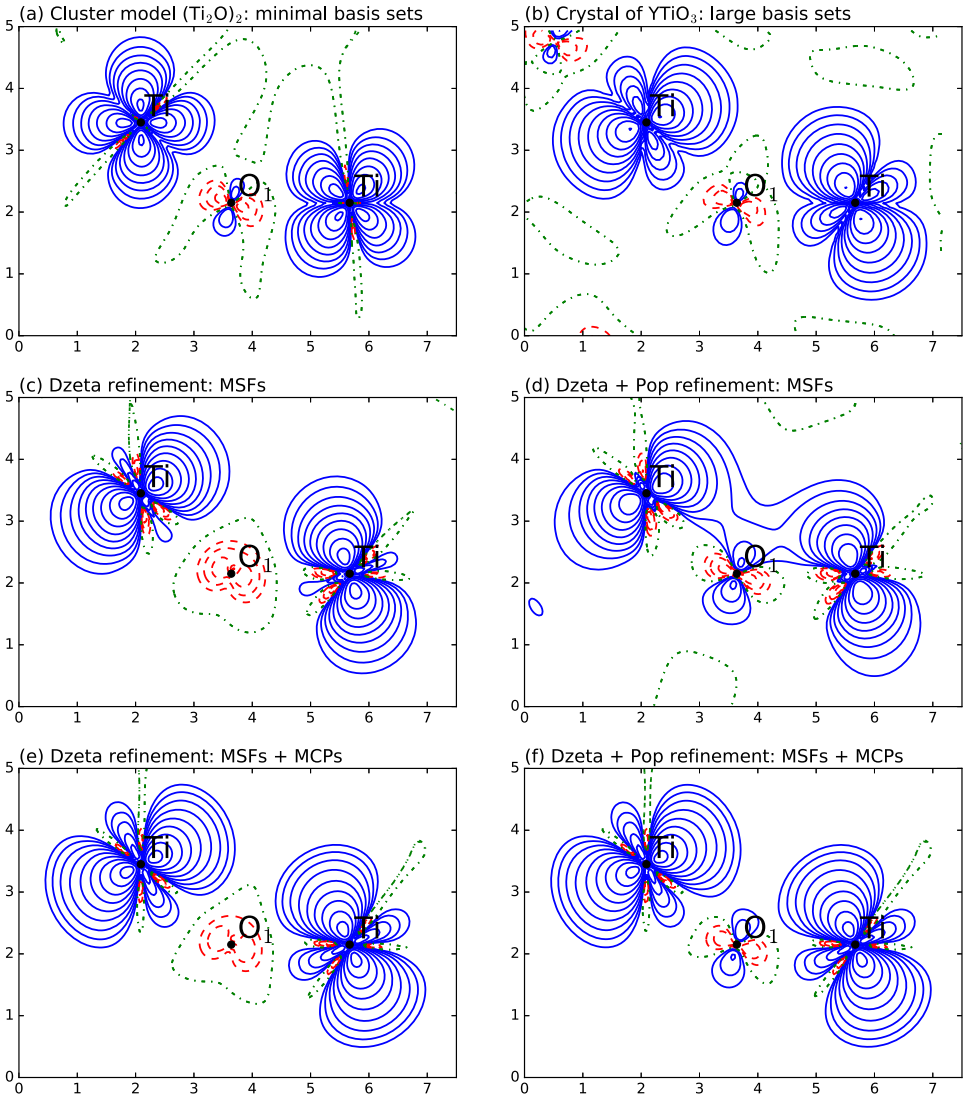

FIG. 2. Spin density maps in the Ti–O_1–Ti plane. Upper panel: Computed spin-resolved electron densities for $(Ti_2O)_2$ (a) and $YTiO_3$ (b) systems. Second panel: Maps of the Dzeta (c) and Dzeta + Pop (d) refined spin density with respect to the MSFs only. Lower panel: the same as the second panel but obtained by means of the joint refinement strategy (MSFs + MCPs). Contours at intervals of $\pm 0.01 \times 2^n \mu_B$ Å^{-3} (n = 0-12): positive and negative contours are blue solid lines and red dashed lines, respectively. Neutral contours are green dashed-dotted lines.

To optimize the set of the exponent coefficients $\{\zeta\}$, the quantity $C(\chi^2) = \sum_Y \log(\chi^2_Y)$[19] is minimized by means of the MINUIT code.[48] In this work, Y stands for two pseudo-experiments, the polarized neutron (PN) diffraction and the magnetic Compton (MC) scattering. Therefore the quantity $C(\chi^2)$ is defined as follows:

$$C\left(\chi^2\left(\{\zeta\}\right)\right) = \log\left(\chi^2_{PN}\left(\{\zeta\}\right)\right) + \log\left(\chi^2_{MC}\left(\{\zeta\}\right)\right). \quad (12)$$

Once the optimal basis functions have been obtained, the spin population matrix is adjusted (denoted "Pop refinement") by varying the molecular occupation numbers for a selection of states and for each spin configuration,

$$n_i^\sigma = n_{i,0}^\sigma + \delta n_i^\sigma, \quad (13)$$

where $n_{i,0}^\sigma$ is the initial molecular occupation number of the ith state and $\sigma = [\uparrow, \downarrow]$. The variation of occupation numbers is performed under the N-representability conditions

$$\begin{cases} 0 \le n_i^\sigma \le 1 & , \\ \sum_{i=1}\left(n_i^\uparrow + n_i^\downarrow\right) = N_{electron}, \\ \sum_{i=1}\left(n_i^\uparrow - n_i^\downarrow\right) = N_{spin} & . \end{cases} \quad (14)$$

The first condition reflects the Pauli principle, while the second and the third represent the electron number conservation and the spin number conservation, respectively. To find the best molecular occupation numbers $\{n\}$ for each spin state configuration, the following quantity is minimized using the MINUIT code:[48]

$$\begin{aligned} C\left(\chi^2\left(\{n\}\right)\right) = \log\left(\chi^2_{PN}\left(\{n\}\right)\right) + \log\left(\chi^2_{MC}\left(\{n\}\right)\right) \\ - \mu_1\left(\sum_{i=1} n_i^\uparrow - N_{electron}^\uparrow\right) \\ - \mu_2\left(\sum_{i=1} n_i^\downarrow - N_{electron}^\downarrow\right), \end{aligned} \quad (15)$$

where μ_1, μ_2 are Lagrange multipliers.

A periodic calculation of $YTiO_3$ using the CRYSTAL14 package[49–51] was conducted to generate pseudo-experimental data (MSFs and MCPs). This calculation is performed by means of the Density Functional Theory (DFT) and the PBE0-1/3[52] of hybrid exchange and correlation functional. In order to better account for the diffuse and polarization effects, an extended basis set pob-TZVP[53] was used. In the present work,

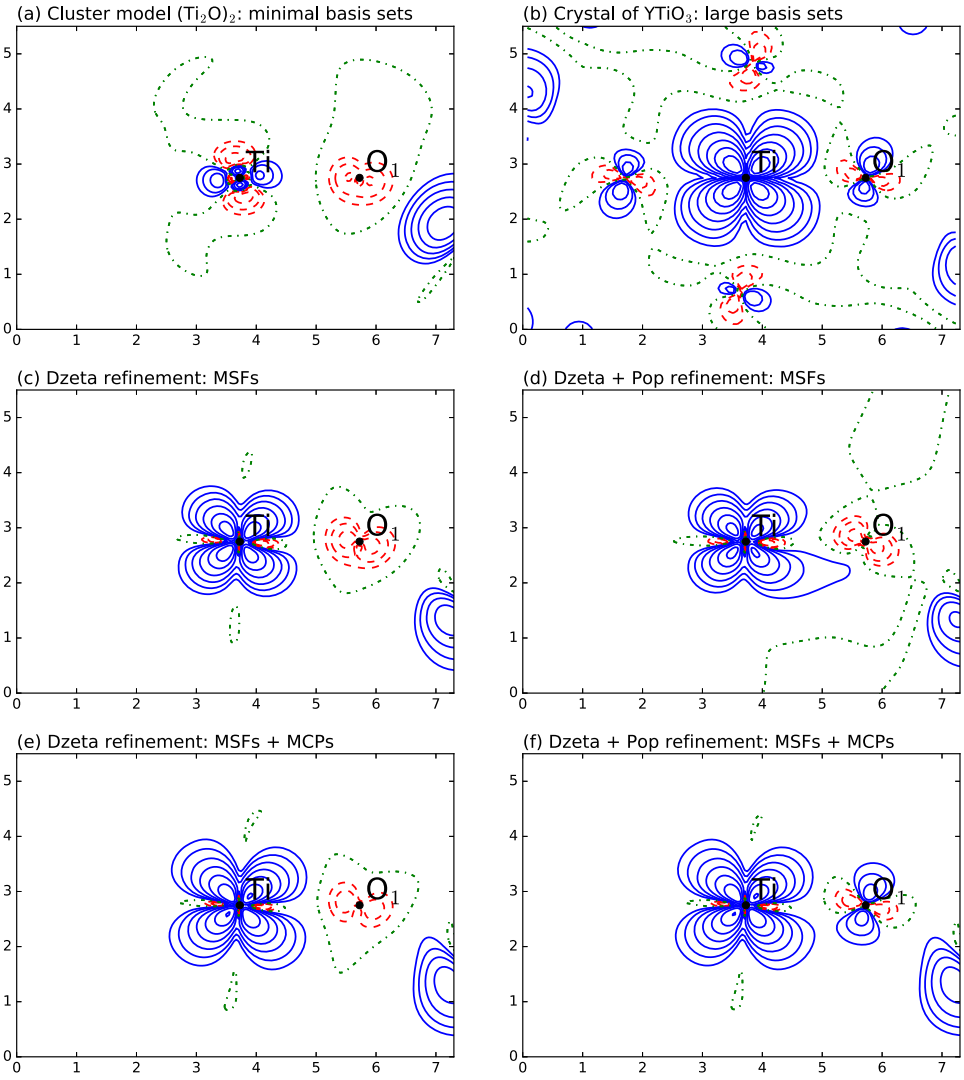

FIG. 3. Spin density maps in the Ti–O_1–O_2' plane. Upper panel: Computed spin resolved electron densities for $(Ti_2O)_2$ (a) and $YTiO_3$ (b) systems. Second panel: Maps of the Dzeta (c) and Dzeta + Pop (d) refined spin density with respect to the MSFs only. Lower panel: The same as the second panel but obtained by means of the joint refinement strategy (MSFs + MCPs). Contours at intervals of $\pm 0.01 \times 2^n \mu_B$ Å^{-3} (n = 0-12): positive and negative contours are blue solid lines and red dashed lines, respectively. Neutral contours are green dashed-dotted lines.

500 MSFs and 12 MCPs were computed. Gaussian distributions of noise corresponding to usual statistical errors are added to the resulting MSFs and MCPs. For the MSF data, the error bar of each point corresponds to 10% of its corresponding MSF amplitude. For the MCP data, the error bar of each point corresponds to the square root of its corresponding MCP amplitude.

III. RESULTS AND DISCUSSIONS

The joint refinement against polarized neutron diffraction and directional magnetic Compton scattering pseudo-data gives access to the description of the unpaired electron in both momentum and position spaces. Polarized neutron diffraction focuses on the local distribution of the electron density in the position space, while magnetic Compton scattering is more sensitive to the delocalized unpaired electron distribution by considering their behavior in the momentum space. In this paper, a simple cluster model $(Ti_2O)_2$ is proposed to partially represent the crystalline 3-D periodic $YTiO_3$ system. This model is used to emphasize the role played by O_1 in the ferromagnetic coupling along the Ti–O_1–Ti path. We present here the results of such a joint refinement model of 1-*SRDM* using the corresponding pseudo-experimental data (MSFs and MCPs). The starting MSF and MCP values are derived from a molecular calculation within a minimal basis set (6-31G),[38–46] to allow for a fair estimate of the accuracy of the joint refinement process. The initial molecular calculated spin density in the Ti–O_1–Ti plane is displayed in Fig. 2 for comparison with the results of joint refinements on pseudo-experimental data and the periodic calculation. In order to illustrate the potential benefits brought by a joint refinement, we also present the resulting spin density from refinement on MSFs only. By comparing the molecular [Fig. 2(a)] and

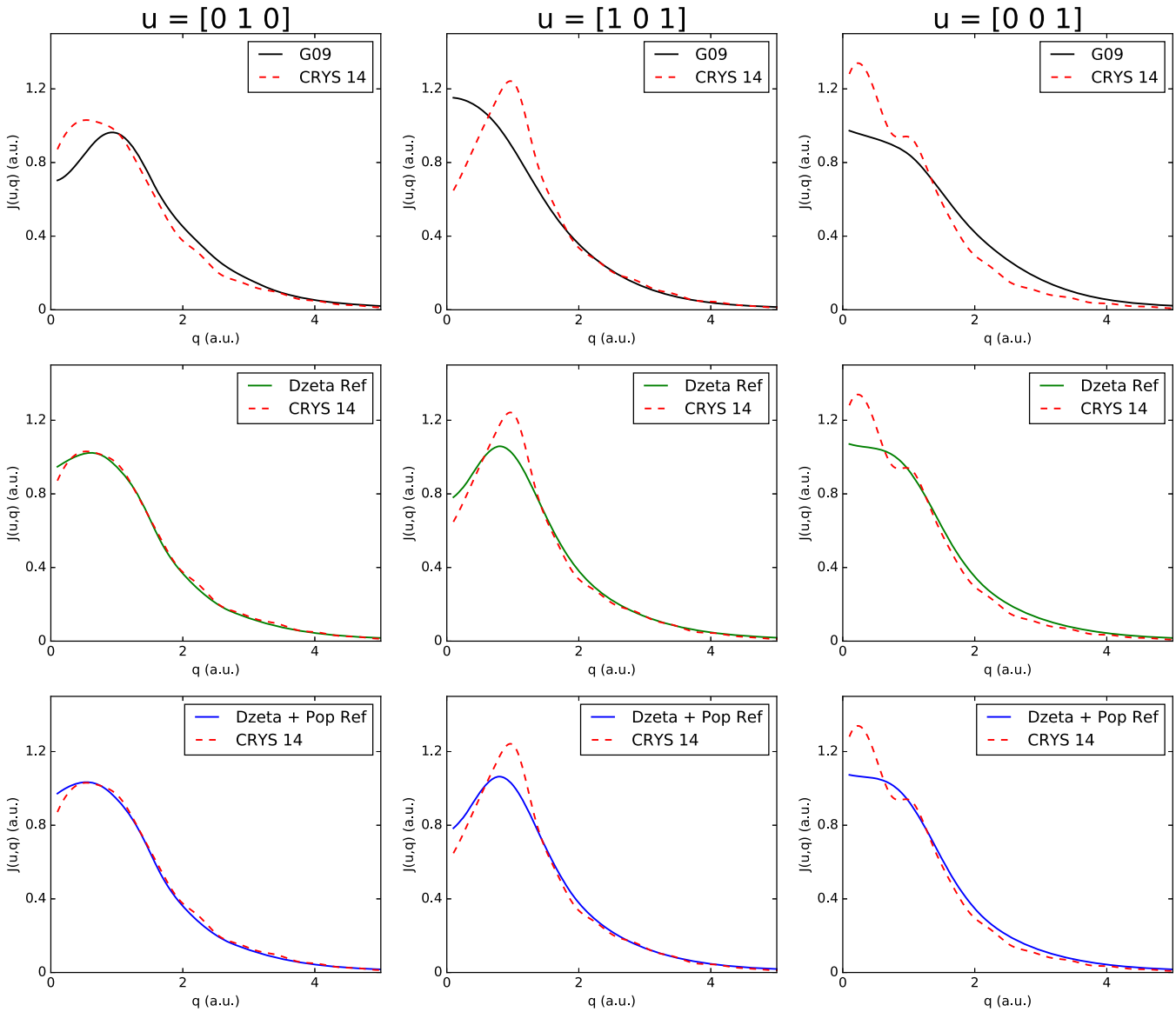

FIG. 4. MCPs computed on the following directions [0 1 0], [1 0 1], and [0 0 1] as a function of the momentum q. For each direction, the resulting MCPs from the periodic calculation (CRYS 14, red dashed lines) are compared to resulting MCPs from the molecular calculation (G09, black solid lines), Dzeta refinement (Dzeta Ref, green solid lines), and Dzeta + Pop refinement (Dzeta + Pop Ref, blue solid lines).

the periodic [Fig. 2(b)] spin electron distributions, differences appear clearly around the Ti atoms. The weak spin electron distribution around the O_1 atom is slightly different. These differences are due to a combination of three effects: (i) improved basis sets, (ii) use of DFT rather than HF, and (iii) use of "real" crystal field rather than "embedded charges." Our results show that the MSFs' input improve the spin densities but remain at variance with the periodic results. The positive lobes around Ti atoms now have the same orientation as in the periodic calculation results. The spin electron distribution on the O_1 atom is different in amplitude from those of periodic calculations. However, by combining MCPs and MSFs, the refined spin densities on Ti and O_1 are consistent with the pseudo-experimental results. The spin resolved electron distribution around the Ti atoms has significantly improved by means of the basis function optimisations (Dzeta refinement). Additionally, the adjustment of the molecular orbital occupation numbers (Pop refinement) improves the spin electron distribution on the O_1 atom. Figure 3 shows a comparison of refined spin densities in the Ti–O_1–O_2' plane with those obtained from the initial molecular and reference periodic calculations. The molecular [Fig. 3(a)] and the periodic [Fig. 3(b)] spin electron distributions around Ti and O_1 atoms are clearly different. Our refinement results show that the MSFs information mainly improves the spin densities on the Ti atom, but it remains in disagreement with pseudo-experimental spin densities. However, the spin densities after refinement against MSFs and MCPs now compare very well with the reference result. Similarly, the rescaling of the basis functions taking into account the diffuse effect improves the spin electron distribution on the Ti atom, whereas the spin electron distribution on the O_1 atom is improved by means of the variation of molecular occupation numbers. The spin electron distributions around O_1 and Ti atoms in this plane are in agreement with the theoretical and experimental results.[17] For both planes, it is shown that the joint refinement model gives more accurate results than the refinement on MSFs only. The distribution of 3*d* orbitals of the Ti atoms in both planes obtained from the joint refinement model is consistent with the periodic results. This confirms that the magnetic interaction between the neighboring Ti atoms is governed by the superexchange process mediated by the O_1 atom.

We now compare the spin-resolved electron density of the Ti and O_1 atoms in momentum space. In this work, the joint refinement of spin resolved electron density is performed with respect to 12 directions of MCPs. Figure 4 displays a comparison of the molecular and the refined MCPs with the pseudo-experimental data for three directions [0 1 0], [1 0 1], and [0 0 1]. Differences between computed molecular and periodic MCPs are clearly seen for all directions. The Dzeta + Pop refinement against MCPs and MSFs show a clear and significant improvement in the reproduction of pseudo-experimental results mainly in the [0 1 0] direction. As can be clearly seen, the resulting MCPs are mostly driven by the variation of the basis functions, additional refinement of the population does not change very much the results. For the [0 1 0] direction, the refined MCP is the most accurate result because this direction corresponds approximately

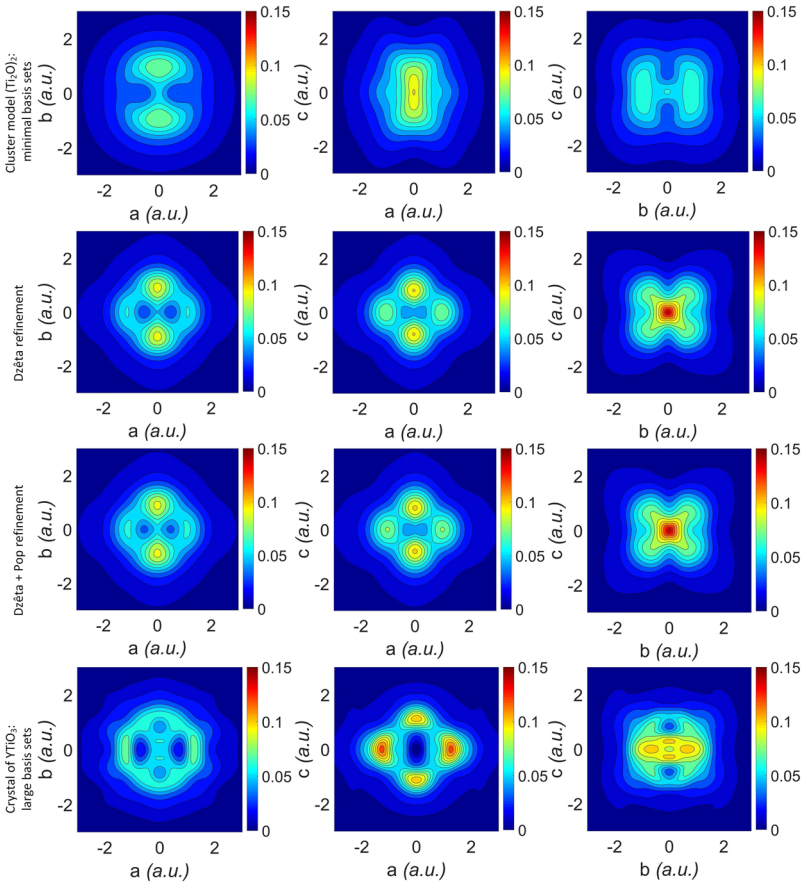

FIG. 5. Reconstructed spin resolved electron density in momentum space (in a.u.), projected onto the three main crystallographic planes: the left column corresponds to the *ab* plane, the middle to the *ac* plane and the right to the *bc* plane. Upper panel: Reconstructed spin density obtained from the molecular calculation. Second and third panels correspond to the Dzeta and Dzeta + Pop refinement, respectively. Lower panel: Reconstructed spin density obtained from the periodic calculation.

to the Ti–O_1–Ti interactions. The resulting MCP from joint refinement along the [1 0 1] direction also shows a strong variation around q = 1 a.u., in agreement with the theoretical and experimental results.[18] However, the molecular calculations exhibit an isotropic distribution in this plane because this direction lies parallel to Ti–O_2–Ti path and the O_2 atom is excluded from our model. This shows the accuracy and performance of our model. For the [0 0 1] direction, the resulting MCP is improved mainly by the variation of the basis functions, but it remains in disagreement with the pseudo-experimental MCP. To evaluate the extent of the accuracy of the refined MCPs for all other directions, the reconstructed 2-D momentum spin density is now presented. This density has been reconstructed from all MCPs using the inverse Fourier transform,

$$n(\mathbf{p}) = \frac{1}{(2\pi)^3} \int B(\mathbf{r}) e^{i\mathbf{p}\cdot\mathbf{r}} d\mathbf{r}, \tag{16}$$

where $B(\mathbf{r})$ is the autocorrelation function for each particular direction, the latter is related to MCPs by

$$B(\mathbf{u}, t) = \int J(\mathbf{u}, q) e^{-iq\cdot t} dq, \tag{17}$$

where $\mathbf{u}$ is the unit vector collinear to the scattering vector and t refers to the relative position between two locations of the same particle along this direction. The spin electron density in momentum space, reconstructed from 12 MCPs,

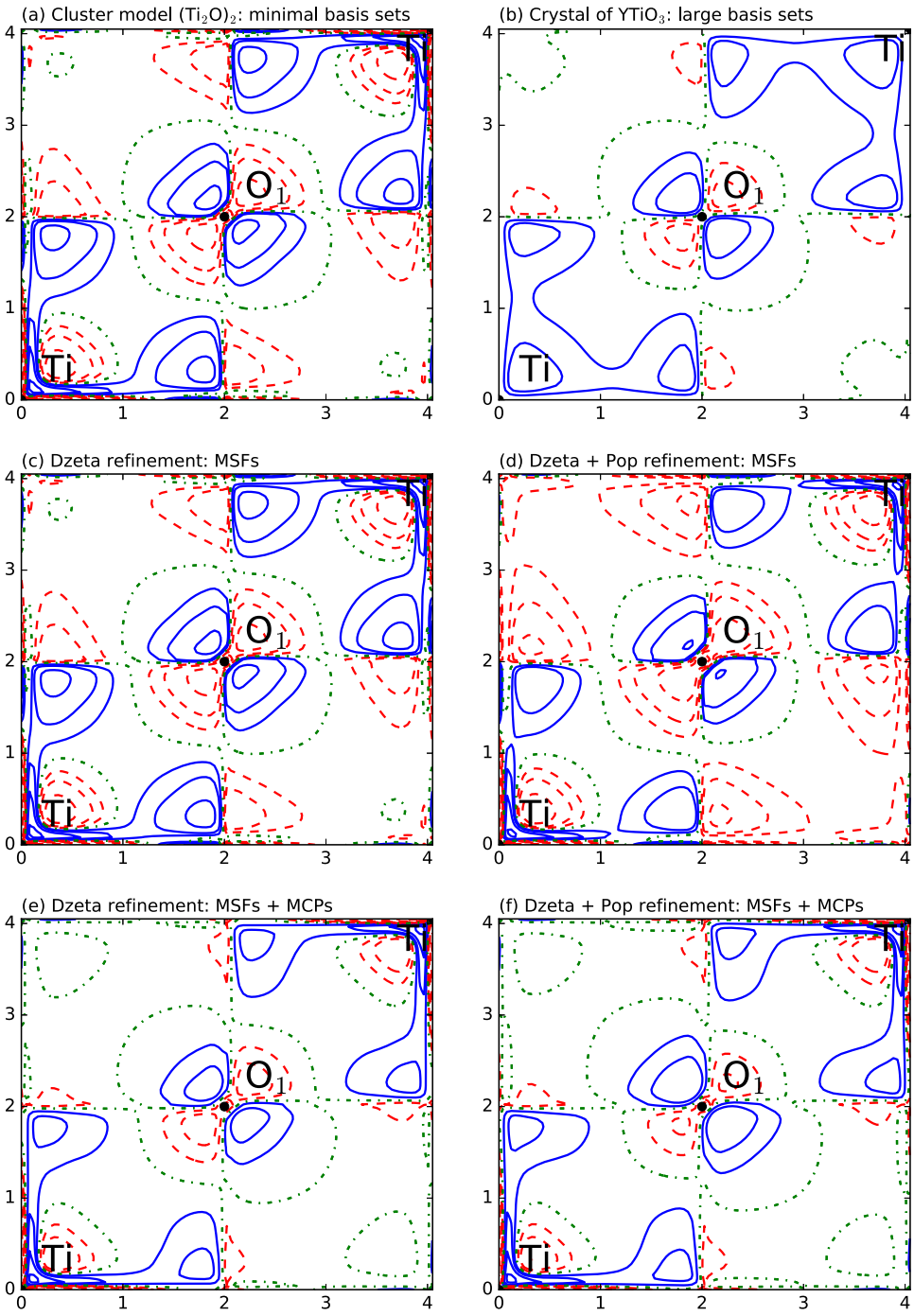

FIG. 6. 1-*SRDM* $\Gamma^{(1)}(\mathbf{r}, \mathbf{r}')$ along the Ti–O_1–Ti bonding. The upper panel shows the molecular (a) and periodic (b) computation of the 1-*SRDM*. The second panel shows the 1-*SRDM* after a Dzeta (c) and Dzeta + Pop (d) refinement relative to the MSFs only. The lower panel is the same as the second panel, but by means of the joint refinement (MSFs + MCPs). Contours at intervals of $\pm 0.01 \times 2^n \mu_B$ Å^{-3} (n = 0-20): positive and negative contours are, respectively, blue solid lines and red dashed lines, and neutral contours are green dashed lines.

is projected onto three main crystallographic planes, *ab*, *ac*, and *bc*. Figure 5 shows such reconstructed magnetic momentum densities from molecular and periodic calculations for comparison with the results from a refined model against pseudo-experimental data. By comparing the first and the last panels, differences are clearly seen between the molecular and the periodic magnetic momentum distributions. Our results show that the spin-resolved electron densities of the three planes in the momentum space are strongly affected by the variation of the basis functions. However, the variation of the molecular occupation numbers makes hardly any change to the momentum spin densities. The joint refinement model gives satisfactory results compared with the pseudo-experimental data for the *ac* plane and figures displaying the density in planes *ab* and *bc* do not exhibit a similar level of agreement. This is because the *ac* plane represents mainly the Ti–O_1 interactions, while the other planes are dominated by the interactions between Ti and O_2 atoms, with the latter being excluded in our model.

Both $\rho(\mathbf{r})$ and $n(\mathbf{p})$ are thus spin electron density descriptions in different representations. They can be connected through the 1-*SRDM* which contains all information on the one-electron level. Figure 6 shows a comparison between the resulting 1-*SRDM* from joint refinement and those obtained from molecular and periodic calculations. By comparing the molecular and the periodic calculations of 1-*SRDM*, differences are clearly seen between molecular and periodic maps in diagonal and off-diagonal regions. The spin densities on the O_1 and Ti atoms are modified by the MSFs information, but remain at variance with pseudo-experimental results. However, the supplementary data of MCPs to MSFs result in a 1-*SRDM* much closer to the periodic results in both the diagonal and off-diagonal regions. This shows that MCPs have a strong impact not only on the off-diagonal regions but also on its diagonal parts and MSFs made a slight change to the off-diagonal regions of the 1-*SRDM*. The comparison of the 1-*SRDM* maps obtained from Dzeta and Dzeta + Pop refinements relative to MSFs + MCPs confirms that the corrections made to the 1-*SRDM* are due to the variation of the basis functions. However, the comparison of the 1-*SRDM* maps obtained from Dzeta and Dzeta + Pop refinements relative to MSFs only shows that the corrections made to the 1-*SRDM* are due to the variation of the molecular orbitals occupation numbers. We deduce that the variation of the basis functions is affected by the MCP information, whereas the molecular orbitals occupation numbers are optimised by the MSF information.

IV. CONCLUSIONS

In this work, we studied the electronic and the magnetic properties of the crystal $YTiO_3$ from a simple cluster model $(Ti_2O)_2$ with very limited basis sets. To reproduce these space dependent properties, the entire 1-*SRDM* of $(Ti_2O)_2$ was refined with respect to the MSFs and the MCPs simultaneously using the joint refinement strategy. This model is implemented as a post-processing of a molecular *ab initio* package. The pseudo-experimental data MSFs and MCPs are generated from periodic calculations by means of the CRYSTAL 14 packages. We have shown that the joint refinement model gives more accurate results than the refinement against MSFs only. We have confirmed that the MCPs have a strong effect on both diagonal and off-diagonal regions of 1-*SRDM*, while the MSFs affect the diagonal regions and made a slight change to the off-diagonal regions. The spin electron distributions on the O_1 and Ti atoms are in good agreement with the theoretical and experimental spin densities. The O_1 atom presents a small magnetic moment and governs a ferromagnetic superexchange interactions between the neighboring Ti atoms. Our results show the following: in position space, the rescaling of the basis functions improves the spin electron distribution on Ti atom, whereas the spin electron distribution on the O_1 atom is improved by means of the variation of molecular occupation numbers. In momentum space, the spin electron distribution is strongly affected by the variation of the basis functions and hardly changed by the variation of the molecular occupation numbers. We have deduced that the basis functions are rescaled by means of MCP and MSF information, while the molecular orbital occupation numbers are mainly optimized by the MSFs.

ACKNOWLEDGMENTS

This work was financed by the French National Research Agency (ANR) project MTMED (Multi Techniques Modeling of Electron Densities). This work was performed using HPC resources from the 'Mésocentre' computing center of CentraleSupélec and École Normale Supérieure Paris-Saclay supported by CNRS and Region Île-de-France (http://mesocentre.centralsupelec.fr/). We are greatly indebted to Julie McDonald for careful reading of this paper.

[1] I. V. Solovyev, New J. Phys. **11**, 093003 (2009); e-print arXiv:0906.2035 [cond-mat.str-el].
[2] P. J. Baker, T. Lancaster, S. J. Blundell, W. Hayes, F. L. Pratt, M. Itoh, S. Kuroiwa, and J. Akimitsu, J. Phys.: Condens. Matter **20**, 465203 (2008).
[3] X. Yang and G. Wu, Europhys. Lett. **117**, 27004 (2017).
[4] A. C. Komarek, H. Roth, M. Cwik, W.-D. Stein, J. Baier, M. Kriener, F. Bourée, T. Lorenz, and M. Braden, Phys. Rev. B **75**, 224402 (2007).
[5] J. R. Hester, K. Tomimoto, H. Noma, F. P. Okamura, and J. Akimitsu, Acta Crystallogr., Sect. B: Struct. Sci. **53**, 739 (1997).
[6] M. Mochizuki and M. Imada, New J. Phys. **6**, 154 (2004).
[7] H. Sawada and K. Terakura, Phys. Rev. B **58**, 6831 (1998).
[8] J. Choukroun, Phys. Rev. B **84**, 014415 (2011).
[9] M. Itoh and M. Tsuchiya, in *Proceedings of the International Conference on Magnetism (ICM 2000)* [J. Magn. Magn. Mater. **226-230**, 874 (2001)].
[10] C. Ulrich, G. Khaliullin, S. Okamoto, M. Reehuis, A. Ivanov, H. He, Y. Taguchi, Y. Tokura, and B. Keimer, Phys. Rev. Lett. **89**, 167202 (2002).
[11] J. Akimitsu, H. Ichikawa, N. Eguchi, T. Miyano, M. Nishi, and K. Kakurai, J. Phys. Soc. Jpn. **70**, 3475 (2001).
[12] B. Li, D. Louca, B. Hu, J. L. Niedziela, J. Zhou, and J. B. Goodenough, J. Phys. Soc. Jpn. **83**, 084601 (2014).
[13] H. Nakao, Y. Wakabayashi, T. Kiyama, Y. Murakami, M. v. Zimmermann, J. P. Hill, D. Gibbs, S. Ishihara, Y. Taguchi, and Y. Tokura, Phys. Rev. B **66**, 184419 (2002).
[14] F. Iga, M. Tsubota, M. Sawada, H. B. Huang, S. Kura, M. Takemura, K. Yaji, M. Nagira, A. Kimura, T. Jo, T. Takabatake, H. Namatame, and M. Taniguchi, Phys. Rev. Lett. **97**, 139901 (2006).
[15] M. Ito, N. Tuji, F. Itoh, H. Adachi, E. Arakawa, K. Namikawa, H. Nakao, Y. Murakami, Y. Taguchi, and Y. Tokura, J. Phys. Chem. Solids **65**, 1993 (2004), sagamore XIV: Charge, Spin and Momentum Densities.
[16] N. Tsuji, M. Ito, H. Sakurai, K. Suzuki, K. Tanaka, K. Kitani, H. Adachi, H. Kawata, A. Koizumi, H. Nakao, Y. Murakami, Y. Taguchi, and Y. Tokura, J. Phys. Soc. Jpn. **77**, 023705 (2008).

[17]I. A. Kibalin, Z. Yan, A. B. Voufack, S. Gueddida, B. Gillon, A. Gukasov, F. Porcher, A. M. Bataille, F. Morini, N. Claiser, M. Souhassou, C. Lecomte, J. M. Gillet, M. Ito, K. Suzuki, H. Sakurai, Y. Sakurai, C. M. Hoffmann, and X. P. Wang, Phys. Rev. B **96**, 054426 (2017).
[18]Z. Yan, I. A. Kibalin, N. Claiser, S. Gueddida, B. Gillon, A. Gukasov, A. B. Voufack, F. Morini, Y. Sakurai, M. Brancewicz, M. Itou, M. Itoh, N. Tsuji, M. Ito, M. Souhassou, C. Lecomte, P. Cartona, and J. M. Gillet, Phys. Rev. B **96**, 054427 (2017).
[19]M. Deutsch, N. Claiser, S. Pillet, Y. Chumakov, P. Becker, J. M. Gillet, B. Gillon, C. Lecomte, and M. souhassou, Acta Crystallogr., Sect. A: Found. Crystallogr. **68**, 675 (2012).
[20]M. Deutsch, B. Gillon, N. Claiser, J. M. Gillet, C. Lecomte, and M. Souhassou, IUCrJ **1**, 194 (2014).
[21]N. K. Hansen and P. Coppens, Acta Crystallogr., Sect. A: Found. Crystallogr. **34**, 909 (1978).
[22]J. Schweizer, in *Neutron Scattering from Magnetic Materials*, edited by T. Chatterji (Elsevier, Amesterdam, 2006), Chap. 4.
[23]J. M. Gillet, P. J. Becker, and P. Cortona, Phys. Rev. B **63**, 235115 (2001).
[24]S. Pillet, M. Souhassou, Y. Pontillon, A. Caneschi, D. Gatteschi, and C. Lecomte, New J. Chem. **25**, 131 (2001).
[25]J. M. Gillet, Acta Crystallogr., Sect. A: Found. Crystallogr. **63**, 234 (2007).
[26]A. B. Voufack, N. Claiser, C. Lecomte, S. Pillet, Y. Pontillon, B. Gillon, Z. Yan, J.-M. Gillet, M. Marazzi, A. Genoni, and M. Souhassou, Acta Crystallogr., Sect. B: Struct. Sci., Cryst. Eng. Mater. **73**, 544 (2017).
[27]J. M. Gillet and P. J. Becker, J. Phys. Chem. Solids **65**, 2017 (2004).
[28]J. M. Gillet, C. Fluteaux, and P. J. Becker, Phys. Rev. B **60**, 2345 (1999).
[29]P. O. Löwdin, Phys. Rev. **97**, 1474 (1955).
[30]A. J. Coleman, Rev. Mod. Phys. **35**, 668 (1963).
[31]R. McWeeny, Rev. Mod. Phys. **32**, 335 (1960).
[32]E. R. Davidson, *Reduced Density Matrices in Quantum Chemistry* (Academic Press, New York, 1976).
[33]P. J. Brown, J. B. Forsyth, and R. Mason, Philos. Trans. R. Soc., B **290**, 481 (1980).
[34]P. Coppens, *X-Ray Charge Densities and Chemical Bonding: International Union of Crystallography Texts on Crystallography* (Oxford University Press, 1997), Vol. 4.
[35]W. Weyrich, "One-electron density matrices and related observables," in *Quantum Mechanical Ab-initio Calculation of the Properties of Crystalline Materials*, edited by C. Pisani (Spinger Berlin, 1996), pp. 245–272.
[36]M. J. Cooper, P. E. Mijnarends, N. Shiotani, N. Sakai, and A. Bansil, *X-Ray Compton Scattering* (Oxford University Press, 2004).
[37]S. Gueddida, Z. Yan, and J.-M. Gillet, Acta Crystallogr., Sect. A: Found. Adv. **74**, 131 (2018).
[38]R. Ditchfield, W. J. Hehre, and J. A. Pople, J. Chem. Phys. **54**, 724 (1971).
[39]W. J. Hehre, R. Ditchfield, and J. A. Pople, J. Chem. Phys. **56**, 2257 (1972).
[40]P. C. Hariharan and J. A. Pople, Theor. Chim. Acta **28**, 213 (1973).
[41]P. Hariharan and J. Pople, Mol. Phys. **27**, 209 (1974).
[42]M. S. Gordon, Chem. Phys. Lett. **76**, 163 (1980).
[43]M. M. Francl, W. J. Pietro, W. J. Hehre, J. S. Binkley, M. S. Gordon, D. J. DeFrees, and J. A. Pople, J. Chem. Phys. **77**, 3654 (1982).
[44]R. C. Binning and L. A. Curtiss, J. Comput. Chem. **11**, 1206 (1990).
[45]J.-P. Blaudeau, M. P. McGrath, L. A. Curtiss, and L. Radom, J. Chem. Phys. **107**, 5016 (1997).
[46]V. A. Rassolov, J. A. Pople, M. A. Ratner, and T. L. Windus, J. Chem. Phys. **109**, 1223 (1998).
[47]M. J. Frisch, G. W. Trucks, H. B. Schlegel, G. E. Scuseria, M. A. Robb, J. R. Cheeseman, G. Scalmani, V. Barone, B. Mennucci, G. A. Petersson, H. Nakatsuji, M. Caricato, X. Li, H. P. Hratchian, A. F. Izmaylov, J. Bloino, G. Zheng, J. L. Sonnenberg, M. Hada, M. Ehara, K. Toyota, R. Fukuda, J. Hasegawa, M. Ishida, T. Nakajima, Y. Honda, O. Kitao, H. Nakai, T. Vreven, J. A. Montgomery, J. E. Peralta, F. Ogliaro, M. Bearpark, J. J. Heyd, E. Brothers, K. N. Kudin, V. N. Staroverov, R. Kobayashi, J. Tomasi, M. Cossi, N. Rega, J. M. Millam, M. Klene, J. E. Knox, J. B. Cross, V. Bakken, C. Adamo, J. Jaramillo, R. Gomperts, R. E. Stratmann, O. Yazyev, A. J. Austin, R. Cammi, C. Pomelli, J. W. Ochterski, R. L. Martin, K. Morokuma, V. G. Zakrzewski, G. A. Voth, P. Salvador, J. J. Dannenberg, S. Dapprich, A. D. Daniels, O. Farkas, J. B. Foresman, J. V. Ortiz, J. Cioslowski, and D. J. Fox, GAUSSIAN 09, Revision B.01, Gaussian, Inc., 2009.
[48]F. James, MINUIT Function Minimization and Error Analysis: Reference Manual Version 94.1, 1994.
[49]C. Pisani, *Quantum-Mechanical Ab-initio Calculation of the Properties of Crystalline Materials* (Spinger, Berlin, 1996).
[50]R. Dovesi, R. Orlando, A. Erba, C. M. Zicovich-Wilson, B. Civalleri, S. Casassa, L. Maschio, M. Ferrabone, M. D. La Pierre, P. D'Arco, Y. Noël, M. Causá, M. Rérat, and B. Kirtman, Int. J. Quantum Chem. **114**, 1287 (2014).
[51]R. Dovesi, V. R. Saunders, C. Roetti, R. Orlando, C. M. Zicovich-Wilson, F. Pascale, B. Civalleri, K. Doll, N. M. Harrison, I. J. Bush, P. D'Arco, M. Llunell, M. Causa, and Y. Noel, *CRYSTAL14 User's Manual* (University of Torino, Torino, 2014).
[52]C. A. Guido, E. Brémond, C. Adamo, and P. Cortona, J. Chem. Phys. **138**, 021104 (2013).
[53]M. F. Peintinger, D. V. Oliveira, and T. Bredow, J. Comput. Chem. **34**, 451 (2013).